Composites Science and Technology 218 (2022) 109130

Contents lists available at ScienceDirect

Composites Science and Technology

journal homepage: www.elsevier.com/locate/compscitech

Modelling the in-plane thermoelectric properties of fibre-reinforced multi-directional laminates

P.A. Carraro [a], A.S. Paipetis [b], A. Pontefisso [a], M. Quaresimin [a], L. Tzounis [b], M. Zappalorto [a,*]

[a] University of Padova, Department of Management and Engineering, Stradella San Nicola 3, 36100, Vicenza, Italy
[b] Department of Materials Science and Engineering, University of Ioannina, 45110, Ioannina, Greece

ARTICLE INFO

Keywords:
Thermoelectric properties
Seebeck coefficient
Composite laminates

ABSTRACT

Analytical models are developed for the first time in this work for assessing the in-plane electric, thermal and thermoelectric properties of multi-directional composite laminates based on the lay-up and the ply orthotropic properties. In particular, both the apparent laminate Seebeck coefficients along two orthogonal in-plane directions and the complete coupled thermoelectric constitutive law are obtained.

The analytical relationships developed are then validated against the results obtained from a bulk of Finite Element (FE) analyses and against both experimental data taken from the literature and the results from an ad hoc experimental campaign carried out in the present work.

The models developed represent a useful tool for designing composite parts to serve as thermoelectrically-enabled structural elements capable of harvesting thermal energy and converting it into electrical, as for instance from heat dissipation found in several applications.

1. Introduction

Composite materials are increasingly adopted for structural components in aircrafts, as well as other transportation means. Given the safety and reliability requirements that such structures need to satisfy, knowing the health state of the most critical components throughout the entire lifetime is essential. Structural health monitoring (SHM) of composite parts is currently carried out by means of periodic inspections through several non-destructive techniques (NDT); accordingly, a methodology for carrying out a continuous monitoring would be extremely beneficial in terms of safety, reliability and costs.

Within this context, electrical methods for the Health Monitoring of composite structures were found effective for the damage monitoring of critical components [1–9] but, of course, they are subjected to the availability of an electric power source. An efficient solution is to obtain the required electric power by exploiting the inherent thermoelectric properties of properly designed composite laminates and the thermal gradients arising in several composite components. Thermal gradients are, indeed, typically present in transportation means. They may be a consequence of the energy dissipation into heat, for instance in regions close to the engines. Alternatively, they may result from other heat sources such as the internal thermal conditioning in vehicles or the de-icing system in airplane wings. Such thermal gradients do not have to be constantly present during the service life, as the resulting electric energy can be harvested and used on-demand for health monitoring inspections.

Carbon fibre reinforced polymer (CFRP) composite laminates are known to exhibit a coupled thermoelectric behaviour (known as the Seebeck effect), which makes them suitable for obtaining thermoelectrically-enabled advanced composites [10]. Accordingly, in the presence of a temperature difference, ΔT, between two points of a composite structure, a voltage drop, Δv, is generated. In the open circuit condition, the relationship $\Delta v = s \cdot \Delta T$ holds valid, where s is the Seebeck coefficient.

In view of the captivating possibility of harvesting electric energy from thermal gradients, the thermoelectric properties of composite materials have attracted an increasingly attention in the recent years. For example, detailed experimental characterizations of the thermoelectric behaviour of carbon fibre reinforced polymers can be found, amongst the others, in Refs. [10–14]. On the other hand, comparatively far less attention has been devoted to the development of models to predict the thermoelectric behaviour of composites, probably due to the difficulties related to the coupled and non-linear nature of the constitutive law. Analytical upper and lower boundary solutions for the

* Corresponding author.
E-mail address: michele.zappalorto@unipd.it (M. Zappalorto).

https://doi.org/10.1016/j.compscitech.2021.109130
Received 3 August 2021; Received in revised form 6 October 2021; Accepted 2 November 2021
Available online 6 November 2021
0266-3538/© 2021 The Authors. Published by Elsevier Ltd. This is an open access article under the CC BY-NC-ND license (http://creativecommons.org/licenses/by-nc-nd/4.0/).

Seebeck coefficient of generic composites were obtained in Ref. [15], whereas micromechanics-based models for particulate composites based on classical homogenization schemes can be found in other studies reported in the literature [16–18].

More recently, a set of accurate models for predicting the orthotropic thermoelectric response of unidirectional composites, based on the constituent properties and the fibre volume fraction, was developed and validated by the authors [19]. However, in the engineering practice, multi-directional laminates, with several plies stacked with different orientations, are more likely to occur. This brings to the need of developing a model for assessing the thermoelectric properties of the whole laminate, starting from the lay-up and the single ply properties, the latter to be measured or estimated (as done, for example, in Ref. [19]). To the best of the authors' knowledge, such a model is not available in the literature, so far.

The main aim of this work is to fill this gap, developing a new analytical model for assessing the Seebeck coefficients' matrix and the full in-plane thermoelectric constitutive law of multi-directional laminates, accounting for the laminate configuration and the ply properties. Moreover, a throughout discussion on the influence of edge effects on the thermoelectric properties of finite-size rectangular specimens is carried out, highlighting the existence of three theoretical limit conditions. As a first step of validation, the analytical predictions obtained from the developed models are compared with the results from several numerical analyses carried out on periodic laminate volume elements. Then, to conclude the work, an experimental validation is performed using data taken from the literature as well as data coming from an ad hoc experimental campaign carried out in this work.

2. Analytical models for the bulk laminate properties

Consider a generic unit width laminate made of n layers, each one with thickness h_i and orientation θ_i with respect to the global reference system x,y (Fig. 1). In the following treatise, each ply is treated as homogeneous and orthotropic with, in general, different properties along its longitudinal and transverse directions, identified with the subscripts 1 and 2, respectively. In this section, models for assessing the apparent in-plane thermoelectric properties of the laminate, starting from those of the single layer, are developed. Though the main focus of the present work is on the laminate Seebeck coefficients and the entire coupled thermoelectric constitutive law, the models for predicting the laminate electric and thermal conductivities are reported as well. Indeed, they are necessary for the development of the thermoelectric model and the assessment of the coupled thermoelectric laminate constitutive law.

A fundamental hypothesis at the basis of the analytical derivations is the planarity of the electric and thermal fluxes. This is ensured only in the absence of damage and far from free edges, i.e. in the "bulk" regions of the laminate, where the electric potential and the temperature do not vary along the laminate thickness. Accordingly, each ply is characterised by the same values of the electric field and thermal gradient. An example supporting this hypothesis is shown in Appendix A.

2.1. Apparent electric properties of a laminate

To the authors' best knowledge, an analytical model for calculating the full electric conductivity matrices of a generic laminate has been derived, for the first time, in Ref. [20] and is briefly recalled hereafter, for the sake of completeness.

According to Ref. [20], the bi-dimensional Ohm's law for the i-th orthotropic ply in its material reference system 1,2 can be written as:

$$\begin{Bmatrix} e_1^i \\ e_1^i \end{Bmatrix} = \begin{bmatrix} \rho_1^i & 0 \\ 0 & \rho_2^i \end{bmatrix} \cdot \begin{Bmatrix} j_1^i \\ j_1^i \end{Bmatrix} \rightarrow \begin{Bmatrix} j_1^i \\ j_1^i \end{Bmatrix} = \begin{bmatrix} \sigma_1^i & 0 \\ 0 & \sigma_2^i \end{bmatrix} \cdot \begin{Bmatrix} e_1^i \\ e_1^i \end{Bmatrix} \tag{1}$$

where e_1^i, e_2^i, j_1^i and j_2^i are the electric fields and current densities in the i-th ply along its longitudinal and transverse directions, respectively. ρ_1^i, ρ_2^i, σ_1^i and σ_2^i are the electric resistivities and conductivities of the i-th ply along the same directions.

Let us consider the following resistivity and conductivity matrices in the material reference system of each ply:

$$[\rho^i] = \begin{bmatrix} \rho_1^i & 0 \\ 0 & \rho_2^i \end{bmatrix} \quad [\sigma^i] = \begin{bmatrix} \sigma_1^i & 0 \\ 0 & \sigma_2^i \end{bmatrix} \tag{2}$$

with $[\sigma^i] = [\rho^i]^{-1}$.

The Ohm's law in the global reference system (x,y) for the i-th ply can be instead written as

$$\begin{Bmatrix} e_x^i \\ e_y^i \end{Bmatrix} = [\overline{\rho}^i] \begin{Bmatrix} j_x^i \\ j_y^i \end{Bmatrix} = \begin{bmatrix} \overline{\rho}_{xx}^i & \overline{\rho}_{xy}^i \\ \overline{\rho}_{yx}^i & \overline{\rho}_{yy}^i \end{bmatrix} \begin{Bmatrix} j_x^i \\ j_y^i \end{Bmatrix} \tag{3}$$

$$\begin{Bmatrix} j_x^i \\ j_y^i \end{Bmatrix} = [\overline{\sigma}^i] \begin{Bmatrix} e_x^i \\ e_y^i \end{Bmatrix} = \begin{bmatrix} \overline{\sigma}_{xx}^i & \overline{\sigma}_{xy}^i \\ \overline{\sigma}_{yx}^i & \overline{\sigma}_{yy}^i \end{bmatrix} \begin{Bmatrix} e_x^i \\ e_y^i \end{Bmatrix} \tag{4}$$

where

$$[\overline{\rho}^i] = [T(\theta_i)][\rho^i][T(\theta_i)]^{-1} \tag{5}$$

$$[T(\theta_i)] = \begin{bmatrix} \cos\theta_i & -\sin\theta_i \\ \sin\theta_i & \cos\theta_i \end{bmatrix} \tag{6}$$

and:

$$[\overline{\sigma}^i] = [\overline{\rho}^i]^{-1} \tag{7}$$

As mentioned, there is no potential variation along the thickness of the laminate and the electric fields along x and y are the same for all the plies, which therefore act as resistors in parallel:

$$\begin{Bmatrix} e_x^i \\ e_y^i \end{Bmatrix} = \begin{Bmatrix} e_x \\ e_y \end{Bmatrix} \tag{8}$$

Consider, now, that the laminate is crossed by the global current components per unit width I_x and I_y, along x and y, respectively. Then,

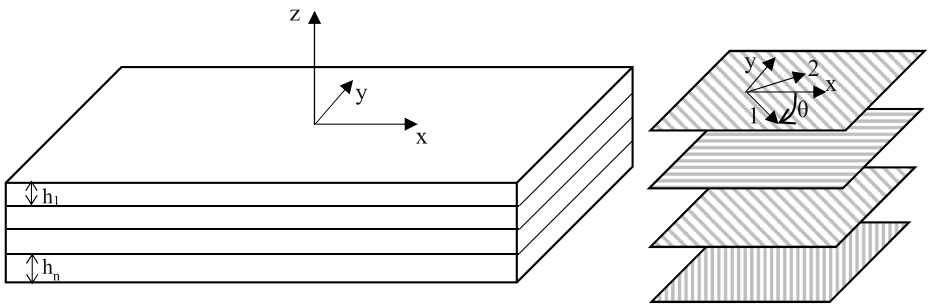

Fig. 1. Laminate geometry and reference systems.

the global charge conservation principle requires that:

$$\begin{Bmatrix} I_x \\ I_y \end{Bmatrix} = \sum_{i=1}^{n} h_i \begin{Bmatrix} j_x^i \\ j_y^i \end{Bmatrix} \tag{9}$$

Substituting Eqs. (4) and (8) into (9), the following relationships are obtained:

$$\begin{Bmatrix} I_x \\ I_y \end{Bmatrix} = [A] \begin{Bmatrix} e_x \\ e_y \end{Bmatrix} = \begin{bmatrix} A_{xx} & A_{xy} \\ A_{yx} & A_{yy} \end{bmatrix} \begin{Bmatrix} e_x \\ e_y \end{Bmatrix}$$
$$\begin{Bmatrix} e_x \\ e_y \end{Bmatrix} = [a] \begin{Bmatrix} I_x \\ I_y \end{Bmatrix} = \begin{bmatrix} a_{xx} & a_{xy} \\ a_{yx} & a_{yy} \end{bmatrix} \begin{Bmatrix} I_x \\ I_y \end{Bmatrix} \tag{10}$$

where

$$[A] = \sum_{i=1}^{n} h_i [\overline{\sigma}^i] \tag{11}$$

and $[a] = [A]^{-1}$.

Eq. (10) represents the electric constitutive law of the laminate in the x,y plane. It can be clearly seen that, even if only an I_x current is applied, the electric fields e_x and e_y are, in general, both different from zero, and vice-versa. This is a consequence of the orthotropic behaviour of the single plies, which becomes anisotropic in the x,y plane when a ply has the fibres rotated of a certain angle with respect to the x direction.

By definition, the apparent laminate conductivity, σ_x, is equal to the ratio between the current density j_x and the electric field e_x, when $I_y = 0$ (i.e. $j_y = 0$). *Vice-versa*, σ_y, is the ratio between j_y and e_y when $I_x = 0$. Accordingly, it results:

$$\sigma_x = \frac{1}{h \cdot a_{xx}}$$
$$\sigma_y = \frac{1}{h \cdot a_{yy}} \tag{12}$$

where h is the total laminate thickness.

It is worth mentioning that these should be considered as bulk laminate properties, representative of the pointwise material response (when the laminate is treated as a homogenized solid). Then, the behaviour of a specimen or a component depends on such properties as well as on the geometry and the boundary conditions, as it will be better discussed in section 4.

2.2. Apparent thermal properties of a laminate

Models for predicting the apparent thermal conductivities along two orthogonal in-plane directions were developed in Refs. [21,22]. However, the full thermal conductivity matrices, accounting for anisotropy-induced couplings between heat fluxes in different directions, were not obtained. Accordingly, in this section the problem is reconsidered, deriving an analytical model to describe the complete thermal behaviour of multi-directional laminates.

To this end, the bi-dimensional Fourier's law for the heat conduction in the i-th orthotropic ply in its material reference system (1,2) can be written as:

$$\begin{Bmatrix} q_1^i \\ q_2^i \end{Bmatrix} = [k^i] \begin{Bmatrix} g_1^i \\ g_2^i \end{Bmatrix} = \begin{bmatrix} k_1^i & 0 \\ 0 & k_2^i \end{bmatrix} \begin{Bmatrix} g_1^i \\ g_2^i \end{Bmatrix} \tag{13}$$

where g_1^i, g_2^i, q_1^i and q_2^i are the temperature gradients and heat fluxes in the i-th ply along its longitudinal and transverse directions, respectively. k_1^i and k_2^i are the thermal conductivities of the i-th ply along the same directions.

The Fourier's law in the global reference system for the i-th ply can be, instead, written as:

$$\begin{Bmatrix} q_x^i \\ q_y^i \end{Bmatrix} = \left[\overline{k}^i\right] \begin{Bmatrix} g_x^i \\ g_y^i \end{Bmatrix} = \begin{bmatrix} \overline{k}_{xx}^i & \overline{k}_{xy}^i \\ \overline{k}_{yx}^i & \overline{k}_{yy}^i \end{bmatrix} \begin{Bmatrix} g_x^i \\ g_y^i \end{Bmatrix} \tag{14}$$

where

$$\left[\overline{k}^i\right] = [T(\theta_i)][k^i][T(\theta_i)]^{-1} \tag{15}$$

As there is no temperature variation along the thickness of the laminate, the layers can be seen as thermal conductors in parallel. In this condition the thermal gradients along x and y are the same for all the plies, so that, for every i-th ply:

$$\begin{Bmatrix} g_x^i \\ g_y^i \end{Bmatrix} = \begin{Bmatrix} g_x \\ g_y \end{Bmatrix} \tag{16}$$

When the laminate is crossed by the global heat transfer components per unit width Q_x and Q_y, along x and y, respectively, the global heat conservation principle reads as:

$$\begin{Bmatrix} Q_x \\ Q_y \end{Bmatrix} = \sum_{i=1}^{n} h_i \begin{Bmatrix} q_x^i \\ q_y^i \end{Bmatrix} \tag{17}$$

Substituting Eqs. (14) and (16) into (17), the following relationships can be obtained:

$$\begin{Bmatrix} Q_x \\ Q_y \end{Bmatrix} = [B] \begin{Bmatrix} g_x \\ g_y \end{Bmatrix} = \begin{bmatrix} B_{xx} & B_{xy} \\ B_{yx} & B_{yy} \end{bmatrix} \begin{Bmatrix} g_x \\ g_y \end{Bmatrix}$$
$$\begin{Bmatrix} g_x \\ g_y \end{Bmatrix} = [b] \begin{Bmatrix} Q_x \\ Q_y \end{Bmatrix} = \begin{bmatrix} b_{xx} & b_{xy} \\ b_{yx} & b_{yy} \end{bmatrix} \begin{Bmatrix} Q_x \\ Q_y \end{Bmatrix} \tag{18}$$

where

$$[B] = \sum_{i=1}^{n} h_i \left[\overline{k}^i\right] \tag{19}$$

and $[b] = [B]^{-1}$.

Eq. (18) represents the thermal constitutive law of the laminate in the x,y plane. It can be clearly seen that, even if only a Q_x component is applied, the gradients g_x and g_y are, in general, both different from zero, and *vice-versa*. Accordingly, a temperature gradient arises in both the in-plane directions, even under a globally unidirectional heat flux. This coupling effect, as well as that relevant to the electric problem, was not considered in the previous models proposed in the literature [21–23], where the full conductivity matrices were not obtained.

By definition, the bulk laminate thermal conductivities, k_x and k_y, are equal to the q_x/g_x and q_y/g_y ratios when $Q_x = 0$ and $Q_y = 0$, respectively. Therefore, they can be expressed as:

$$k_x = \frac{1}{h \cdot b_{xx}}$$
$$k_y = \frac{1}{h \cdot b_{yy}} \tag{20}$$

2.3. Apparent thermoelectric properties of a laminate

In this sub-section, the Seebeck coefficients of a generic multidirectional laminate along the x and y directions, as well as the complete in-plane thermoelectric constitutive law, are obtained.

The coupled constitutive law for the i-th ply, in the material reference system 1,2 reads as:

$$\begin{Bmatrix} j_1^i \\ j_2^i \end{Bmatrix} = [\sigma^i] \begin{Bmatrix} e_1^i \\ e_2^i \end{Bmatrix} + [\sigma^i][s^i] \begin{Bmatrix} g_1^i \\ g_2^i \end{Bmatrix} \tag{21}$$

$$\begin{Bmatrix} q_1^i \\ q_2^i \end{Bmatrix} = [\beta^i][\sigma^i]\begin{Bmatrix} e_1^i \\ e_2^i \end{Bmatrix} + \left([k^i] + [\beta^i][\sigma^i][s^i]\right)\begin{Bmatrix} g_1^i \\ g_2^i \end{Bmatrix} \tag{22}$$

where the $[\sigma^i]$ and $[k^i]$ matrices were previously defined, whereas:

$$[s^i] = \begin{bmatrix} s_1^i & 0 \\ 0 & s_2^i \end{bmatrix}, \quad [\beta^i] = T\cdot[s^i] = \begin{bmatrix} \beta_1^i & 0 \\ 0 & \beta_2^i \end{bmatrix} \tag{23}$$

s_1^i and s_2^i are the longitudinal and transverse Seebeck coefficients of the i-th ply, whereas β_1^i and β_2^i are the Peltier coefficients, namely the Seebeck coefficients times the temperature T.

In the global reference system, the thermoelectric constitutive equations read as:

$$\begin{Bmatrix} j_x^i \\ j_y^i \end{Bmatrix} = [\overline{\sigma}^i]\begin{Bmatrix} e_x^i \\ e_y^i \end{Bmatrix} + [\overline{\sigma}^i][\overline{s}^i]\begin{Bmatrix} g_x^i \\ g_y^i \end{Bmatrix} \tag{24}$$

$$\begin{Bmatrix} q_x^i \\ q_y^i \end{Bmatrix} = \left[\overline{\beta}^i\right][\overline{\sigma}^i]\begin{Bmatrix} e_x^i \\ e_y^i \end{Bmatrix} + \left(\left[\overline{k}^i\right] + \left[\overline{\beta}^i\right][\overline{\sigma}^i][\overline{s}^i]\right)\begin{Bmatrix} g_x^i \\ g_y^i \end{Bmatrix} \tag{25}$$

where:

$$\begin{aligned} [\overline{s}^i] &= \begin{bmatrix} \overline{s}_{xx}^i & \overline{s}_{xy}^i \\ \overline{s}_{yx}^i & \overline{s}_{yy}^i \end{bmatrix} = [T(\theta_i)][s^i][T(\theta_i)]^{-1} \\ \left[\overline{\beta}^i\right] &= \begin{bmatrix} \overline{\beta}_{xx}^i & \overline{\beta}_{xy}^i \\ \overline{\beta}_{yx}^i & \overline{\beta}_{yy}^i \end{bmatrix} = [T(\theta_i)][\beta^i][T(\theta_i)]^{-1} \end{aligned} \tag{26}$$

Considering the charge conservation principle, Eq. (9), together with Eq. (24), one can write

$$\begin{Bmatrix} I_x \\ I_y \end{Bmatrix} = \sum_{i=1}^{n}\begin{Bmatrix} j_x^i \\ j_y^i \end{Bmatrix} h_i = [A]\begin{Bmatrix} e_x \\ e_y \end{Bmatrix} + \sum_{i=1}^{n} h_i[\overline{\sigma}^i][\overline{s}^i]\begin{Bmatrix} g_x \\ g_y \end{Bmatrix} \tag{27}$$

where it has already been considered that the electric field and thermal gradient components are equal for all the plies, according to the iso-potential and iso-temperature hypotheses, valid for the bulk laminate regions.

By definition, the Seebeck coefficients represent the proportionality constants between the electric field and the thermal gradient components, when the global current crossing the laminate is equal to zero. Therefore, by imposing $I_x = I_y = 0$, Eq. (27) can be re-written as:

$$\begin{Bmatrix} e_x \\ e_y \end{Bmatrix} = -[A]^{-1}\sum_{i=1}^{n} h_i[\overline{\sigma}^i][\overline{s}^i]\begin{Bmatrix} g_x \\ g_y \end{Bmatrix} \tag{28}$$

so that the laminate Seebeck matrix, [S] can be expressed as it follows:

$$[S] = \begin{bmatrix} S_{xx} & S_{xy} \\ S_{yx} & S_{yy} \end{bmatrix} = [A]^{-1}\left(\sum_{i=1}^{n} h_i[\overline{\sigma}^i][\overline{s}^i]\right) \tag{29}$$

In general, due to the anisotropy of the material response, it can be deduced that even in the presence of a unidirectional temperature gradient, the electric field components along the in-plane directions are different from zero, thus generating a potential drop along both directions. This happens, in particular, when the laminate lay-up is not balanced, i.e. when, for a given off-axis angle θ different from 0° and 90°, there does not exist a ply oriented at -θ.

The bulk Seebeck coefficients of the laminate along the x and y directions, s_x and s_y, can thus be calculated as:

$$\begin{aligned} s_x &= -\frac{e_x}{g_x}, \quad when \quad g_y = 0 \Rightarrow s_x = S_{xx} \\ s_y &= -\frac{e_y}{g_y}, \quad when \quad g_x = 0 \Rightarrow s_y = S_{yy} \end{aligned} \tag{30}$$

To determine the entire coupled constitutive law, Eq. (29) can be substituted into Eq. (27) so that the first relationship of the thermoelectric law can be written as:

$$\begin{Bmatrix} I_x \\ I_y \end{Bmatrix} = [A]\begin{Bmatrix} e_x \\ e_y \end{Bmatrix} + [A][S]\begin{Bmatrix} g_x \\ g_y \end{Bmatrix} \tag{31}$$

To write the second relationship, the Fourier heat conduction law is considered:

$$\begin{Bmatrix} Q_x \\ Q_y \end{Bmatrix} = \sum_{i=1}^{n} h_i\begin{Bmatrix} q_x^i \\ q_y^i \end{Bmatrix} = [C]\begin{Bmatrix} e_x \\ e_y \end{Bmatrix} + ([B] + [D])\begin{Bmatrix} g_x \\ g_y \end{Bmatrix} \tag{32}$$

[B] was already defined in Eq. (20), whereas matrices [C] and [D] are calculated as:

$$\begin{aligned} [C] &= \left(\sum_{i=1}^{n} h_i\left[\overline{\beta}^i\right][\overline{\sigma}^i]\right) \\ [D] &= \left(\sum_{i=1}^{n} h_i\left[\overline{\beta}^i\right][\overline{\sigma}^i][\overline{s}^i]\right) \end{aligned} \tag{33}$$

Eqs. (31) and (32) represent, therefore, the in-plane coupled thermoelectric laws of the bulk laminate.

3. Periodic finite element analyses and numerical validation

With the aim of validating the analytical models developed in the previous sections, FE analyses on laminates with different stacking sequences were carried out with the code ANSYS 19.2. To eliminate edge effects in the FE results and thus evaluate the bulk laminate properties, periodic boundary conditions were applied to a laminate segment (see the schematic in Fig. 2). The geometrical model consisted of a prism with a base w × w (w being an arbitrary number without any influence given the periodic boundary conditions applied) and a total thickness h, equal to the total laminate thickness. This volume was divided into sub-volumes, each with a thickness h_i, representative of different layers. A uniform and regular mesh was created using brick elements, of which the local reference system was rotated according to the fibre direction of each layer. In Fig. 2, xy represents the laminate plane, whereas z is the through-the-thickness direction; the reference system was centred on the front-right node on the bottom surface, named node N_0. The nodes at the other three vertexes on the bottom surface are referred to as N_1, N_2 and N_3. The four vertical corners are, instead, numbered from 1 to 4, according to Fig. 2. Eventually, opposite faces along directions x and y are called A, B and C, D, respectively.

The periodic boundary conditions and the way to extract the results are reported in the next sub-sections for the electric, thermal and thermoelectric problems.

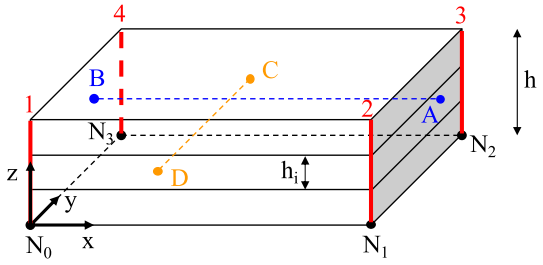

Fig. 2. Schematic of the laminate segment for the FE analyses and nomenclature.

3.1. Electric analyses

The aim of the electric numerical analyses was to estimate the [A] matrix linking the global laminate currents I_x and I_y to the electric field components e_x, e_y (see Eq. (10)). Accordingly, two analyses are required:

i. In the first analysis, through proper boundary conditions, an electric field $e_x = 1$ V/m was applied and e_y was set to zero. In this way, according to Eq. (10), it was possible to calculate $A_{xx} = I_x$ and $A_{yx} = I_y$, where I_x and I_y are the resulting global current components;
ii. In the second analysis, $e_x = 0$ and $e_y = 1$ V/m, so that it was possible to calculate $A_{xy} = I_x$ and $A_{yy} = I_y$.

Once matrix [A] was determined, it was inverted to calculate the apparent laminate conductivities as in Eq. (12).

The global currents per unit width I_x and I_y were calculated from the ANSYS element results as:

$$I_x = \frac{\sum_{i=1}^{n} j_{xi} \cdot Vol_i}{w}, I_y = \frac{\sum_{i=1}^{n} j_{yi} \cdot Vol_i}{w} \tag{34}$$

where j_{xi}, j_{yi} and Vol_i are the x and y direction current densities and the volume of the i-th element, respectively.

The following periodic boundary conditions were applied to obtain $e_x = 1$ V/m and $e_y = 0$:

i. First, the electric potential of node N_0 was set to zero ($v_{N0} = 0$). Then, the following constrain equations were applied between pairs of nodes on faces A, B and C, D, excluding the corners to avoid redundancy issues.

$$\begin{aligned} v_B - v_A &= e_x \cdot w \\ v_D - v_C &= 0 \end{aligned} \tag{35}$$

ii. The following constrain equations were instead applied between corners:

$$\begin{aligned} v_1 - v_2 &= e_x \cdot w \\ v_1 - v_4 &= 0 \\ v_1 - v_3 &= e_x \cdot w \end{aligned} \tag{36}$$

Differently, the boundary conditions for applying $e_x = 0$ and $e_y = 1$ V/m were as follows:

$$\begin{aligned} v_B - v_A &= 0 \\ v_D - v_C &= e_y \cdot w \end{aligned} \tag{37}$$

$$\begin{aligned} v_1 - v_3 &= e_y \cdot w \\ v_1 - v_2 &= 0 \\ v_2 - v_4 &= e_y \cdot w \end{aligned} \tag{38}$$

The SOLID 231 elements of the Ansys library, with one degree of freedom per node (namely the electric potential) were adopted.

3.2. Thermal analyses

The aim of the thermal numerical analyses was to estimate the [B] matrix linking the global laminate heat transfer components Q_x and Q_y to the thermal gradient components g_x, g_y (see Eq. (18)). Accordingly, two analyses are required:

i. In the first analysis, a thermal gradient $g_x = 1$ K/m was applied, keeping g_y equal to zero. Thus, according to Eq. (18), it was possible to calculate $B_{xx} = Q_x$ and $B_{yx} = Q_y$;
ii. In the second analysis, $g_x = 0$ and $g_y = 1$ K/m, so that $B_{xy} = Q_x$ and $B_{yy} = Q_y$.

Once matrix [B] was determined, it was inverted to calculate the apparent laminate thermal conductivities as in Eq. (20).

The global components Q_x and Q_y can be calculated from the ANSYS element results as:

$$Q_x = \frac{\sum_{i=1}^{n} q_{xi} \cdot Vol_i}{w}, Q_y = \frac{\sum_{i=1}^{n} q_{yi} \cdot Vol_i}{w} \tag{39}$$

where q_{xi}, q_{yi} and Vol_i are the x and y direction heat fluxes and the volume of the i-th element, respectively.

The following periodic boundary conditions were applied in order to obtain $g_x = 1$ K/m and $g_y = 0$:

i. First the temperature of node N_0 was set to zero ($T_{N0} = 0$) and then the following constrain equations were applied between pairs of nodes on faces A, B and C, D, again excluding the corners to avoid redundancy issues:

$$\begin{aligned} T_B - T_A &= g_x \cdot w \\ T_D - T_C &= 0 \end{aligned} \tag{40}$$

ii. The following constrain equations were applied, instead, between corners:

$$\begin{aligned} T_1 - T_2 &= g_x \cdot w \\ T_1 - T_4 &= 0 \\ T_1 - T_3 &= g_x \cdot w \end{aligned} \tag{41}$$

Differently, the boundary conditions resulting in $g_x = 0$ and $g_y = 1$ K/m read as:

$$\begin{aligned} T_B - T_A &= 0 \\ T_D - T_C &= g_y \cdot w \end{aligned} \tag{42}$$

$$\begin{aligned} T_1 - T_3 &= g_y \cdot w \\ T_1 - T_2 &= 0 \\ T_2 - T_4 &= g_y \cdot w \end{aligned} \tag{43}$$

The SOLID 90 elements of the Ansys library, with one degree of freedom per node (namely the temperature), were adopted.

3.3. Thermoelectric analyses

Thermoelectric FE analyses were carried out using the Ansys SOLID 226 elements for estimating the apparent laminate Seebeck matrix [S], linking the electric fields e_x and e_y to the thermal gradients g_x, g_y (Eq. (28)). Two degrees of freedom per node are available in the SOLID 226 elements, namely the electric potential and the temperature.

Also in this case, two analyses were carried out:

i. In the first analysis, a thermal gradient $g_x = 1$ K/m was applied setting g_y to zero. In this way, according to Eqs. (28), (29), it was possible to calculate $S_{xx} = -e_x$ and $S_{yx} = -e_y$;
ii. In the second analysis, $g_x = 0$ and $g_y = 1$ K/m, so that $S_{xy} = -e_x$ and $S_{yy} = -e_y$.

The electric field components e_x and e_y were calculated from the ANSYS element results as

$$e_x = \frac{\sum_{i=1}^{n} e_{xi} \times Vol_i}{\sum_{i=1}^{n} Vol_i}, e_y = \frac{\sum_{i=1}^{n} e_{yi} \times Vol_i}{\sum_{i=1}^{n} Vol_i} \tag{44}$$

where e_{xi}, e_{yi} and Vol_i are the x and y direction electric fields and the volume of the i-th element, respectively.

The following periodic boundary conditions were applied to obtain $g_x = 1$ K/m and $g_y = 0$:

i. First, the voltage and the temperature were assigned to node N_0, so that $v_{N0} = 0$ and $T_{N0} = T_0$, where T_0 is arbitrary value (it was chosen equal to 270K in the following analyses, but it was found to have no influence on the final results in terms of Seebeck matrix coefficients).
ii. For the temperature boundary conditions, Eqs. (40), (41) were applied to the faces and the corners, exactly as in the thermal analyses.
iii. As the resulting e_x and e_y components were not known a priori, an electric potential could not be assigned to the vertex nodes. However, the periodicity along the y direction was guaranteed by imposing the following constrain equation for the vertex nodes:

$$v_{N_1} - v_{N_2} = v_{N_0} - v_{N_3} \Rightarrow v_{N_3} + v_{N_1} - v_{N_2} = 0 \tag{45}$$

iv. As the electric field component e_z must be equal to zero, the following conditions were also applied for the nodes on the corners:

$$\begin{aligned} v_1 &= v_{N_0} \\ v_2 &= v_{N_1} \\ v_3 &= v_{N_2} \\ v_4 &= v_{N_3} \end{aligned} \tag{46}$$

v. Then, the following constrain equations were applied between nodes on opposite faces (excluding the corners to avoid redundancy):

$$\begin{aligned} v_B - v_A = v_{N_0} - v_{N_1} \Rightarrow v_{N_1} + v_B - v_A = 0 \\ v_D - v_C = v_{N_0} - v_{N_3} \Rightarrow v_{N_3} + v_D - v_C = 0 \end{aligned} \tag{47}$$

Differently, to obtain a condition according to which $g_x = 0$ and $g_y = 1$ K/m, Eq. (45)-(47) remain valid, and the constrain equations (40), (41) must be substituted by Eqs. (42), (43).

3.4. Comparison with the analytical models

The results of the analytical models were compared with those obtained through electric, thermal and thermoelectric FE analyses carried out on $[0/90/\theta/\text{-}\theta]_s$ and $[0/\theta]_s$ laminates, varying the angle θ between 0° and 90°, applying the boundary conditions discussed in the previous section. It is worth noting that this comprehensive analysis covers common lay-ups used in the engineering practice, such as the quasi-isotropic as well as the cross-ply laminate.

The material properties listed in Table 1 were chosen, typical of a unidirectional carbon/epoxy lamina. In particular, the electrical properties and the transverse thermal conductivities were taken from Ref. [24] (measured for a carbon/epoxy lamina with a fibre volume fraction of 57%). The longitudinal thermal conductivity was estimated based on typical carbon fibre properties [25], whereas the Seebeck coefficients were taken approximately equal to those measured in Ref. [13] for a carbon/epoxy woven fabric in the longitudinal and through-the-thickness directions. 3D FE analyses required the specification of the through-the-thickness properties as well, which were considered equal to those along the transverse direction. The single ply thickness was set equal to 0.5 mm.

The comparison between the analytical and numerical results in terms of electric and thermal conductivities, Seebeck coefficient and the coupling coefficients is shown in Fig. 3. Among these, A_{xy} and B_{xy} were normalised to the laminate thickness h, thus making them independent of this parameter. As evident, there is a perfect agreement between the two solutions, confirming that the analytical formulations provided in section 2 are exact and provide the same results as FE analyses carried out with proper periodic boundary conditions, reproducing the bulk laminate behaviour.

Table 1
Ply-level material properties for the numerical validation.

σ_1 [S/m]	σ_2 [S/m]	k_1 [W/(m·k)]	k_2 [W/(m·k)]	s_1 [μV/K]	s_2 [μV/K]
22000	56	1.7	0.87	−4	−2

It is also interesting to note that the variation in the laminate Seebeck coefficient, s_x, is very limited for the investigated laminate configurations. This is because the longitudinal electric conductivity is much higher that the transverse one (about three orders of magnitude in this case). It is easy to verify that, in these conditions, the laminate Seebeck coefficient obtained through Eqs. (11) and (30) results very close to that along the longitudinal direction.

The trends of the coupling coefficients for the $[0/\theta]_s$ laminate are shown in Fig. 3d, where it can be noted that A_{xy} and B_{xy} have a symmetric behaviour with respect to the case $\theta = 45°$, for which a peak value is reached. Differently, S_{xy} is not symmetric and has, approximatively, a peak value for an off-axis angle $\theta = 6°$.

4. Edge effects

4.1. Preliminary considerations

The analytical solutions presented in section 2 were conceived for calculating the bulk thermoelectric properties of a laminate. It is important to remind that one of the basic assumptions in the mathematical treatise of the problem was the uniformity of the electric field and thermal gradient components along the thickness, ensuring the planarity of the fluxes. As shown in Appendix A, this is true far from free edges and in the absence of intra- and inter-ply damage.

Consider, for instance, the case of a rectangular specimen with a length L and width w, subjected to a potential or temperature difference between the two opposite faces along the x-direction (Fig. 4). As discussed also in Refs. [21,23], the electric and thermal response of the specimen is influenced by edge effects. However, it is not clear from the available literature that such edge effects have a twofold nature:

i. Geometry-induced effects, related to the L/w ratio (Type-I edge effects from now on);
ii. Material property-induced edge effects, related to the material property mismatch between different layers and the w/h ratio (Type-II edge effects from now on);

4.2. Type-I edge effects

Regarding the type-I edge effects, two extreme scenarios can be depicted. For the limiting case of long and narrow specimen ($L \gg w$), the global current and heat power per unit width crossing the laminate along y are almost negligible in the whole laminate ($I_y \cong Q_y \cong 0$). Indeed, close to insulating edges these quantities are null, but as the laminate is very narrow, the condition $I_y \cong Q_y \cong 0$ is approximately verified through the entire laminate width.

Accordingly, the apparent electric and thermal conductivities measured on the rectangular specimen along the x-direction can be calculated as:

$$\sigma^{\infty}_{x,s} = \frac{I_x}{\Delta V_x}\frac{L}{h} = \frac{1}{h \cdot a_{xx}} \tag{48}$$

$$k^{\infty}_{x,s} = \frac{Q_x}{\Delta T_x}\frac{L}{h} = \frac{1}{h \cdot b_{xx}} \tag{49}$$

Although conceptually different from the bulk laminate properties predicted by Eqs. (12) and (20), the specimen conductivities in this case can be calculated with the same formulation, since $I_y \cong Q_y \cong 0$ (see also the definition of laminate conductivities reported in Section 2).

For calculating the apparent Seebeck coefficient of the specimen, the open circuit state ($I_x = 0$) is considered together with $I_y = Q_y = 0$ because of the narrow specimen. Under these conditions, taking advantage of Eqs. (31), (32), the Seebeck coefficient of the specimen in the x-direction reads as:

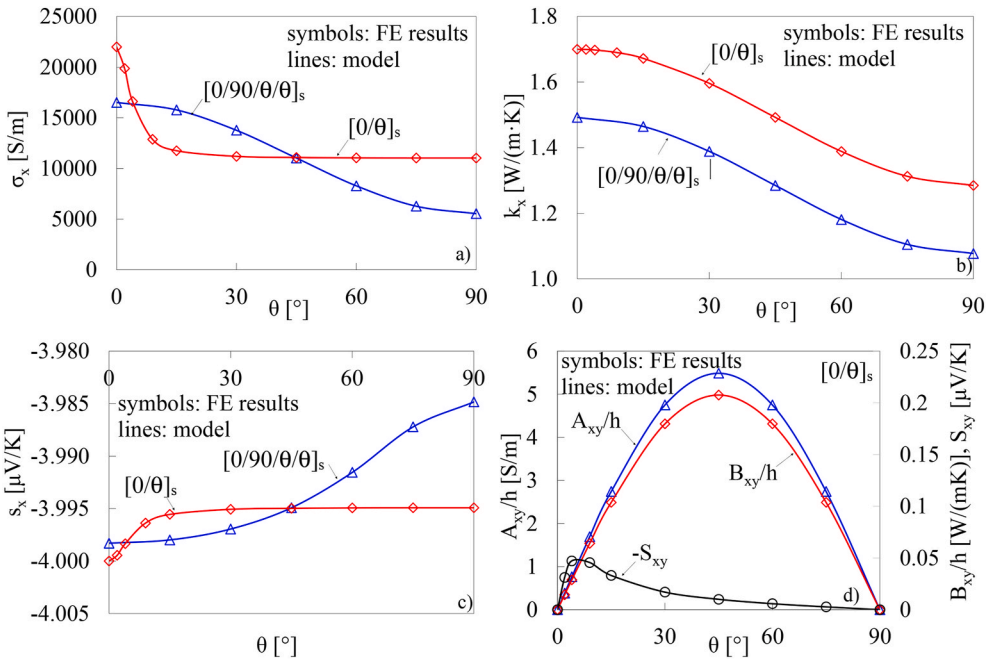

Fig. 3. Comparison between the analytical model and the FE analyses in terms of a) electric and b) thermal conductivity, c) Seebeck coefficient and d) coupling coefficients.

$$s_{x,s}^{\infty} = -\frac{\Delta V_x}{\Delta T_x} = \frac{S_{xx} - S_{xy}\frac{C_{xy}S_{xy}+B_{xy}+D_{xy}}{C_{yy}S_{yy}+B_{yy}+D_{yy}}}{1 + S_{xy}\frac{C_{xy}}{C_{yy}S_{yy}+B_{yy}+D_{yy}}} \tag{50}$$

Accordingly, the Seebeck coefficient measured through a long and narrow specimen does not correspond to the laminate bulk coefficient s_x, as given in Eq. (30), unless the laminate has a balanced lay-up, for which $S_{xy} = 0$. According to Eq. (50) the specimen Seebeck coefficient depends on the temperature through the [C] and [D] matrices. This dependence is very weak in a wide range of operating temperatures, with negligible variations changing the temperature from −200 to 200 °C.

Differently, for short and large specimens ($L \ll w$), the global electric and thermal fluxes along the y-direction are not negligible, as a big portion of the laminate width is sufficiently far from the free edges. In this limit case, the y-direction electric field and thermal gradient, e_y and g_y, tend to zero. Accordingly, exploiting Eqs. (10), (18), the specimen conductivities along the x-direction can be simply calculated as:

$$\sigma_{x,s}^{0} = \frac{I_x}{\Delta V_x}\frac{L}{h} = \frac{A_{xx}}{h} \tag{51}$$

$$k_{x,s}^{0} = \frac{Q_x}{\Delta T_x}\frac{L}{h} = \frac{B_{xx}}{h} \tag{52}$$

It is evident that in the case of unbalanced laminates with $L \ll w$, the specimen conductivities differ from the bulk laminate properties, as they were calculated assuming a condition in which the electric and thermal fluxes along the y-direction were equal to zero. Conversely, for balanced lay-ups, Eqs. (51), (52) give the same results of Eqs. (48), (49). Accordingly, the type-I edge effects affect the behaviour of unbalanced specimens only, namely laminates with a non-symmetric distribution of off-axis plies with respect to the excitation direction, including unidirectional off-axis plies.

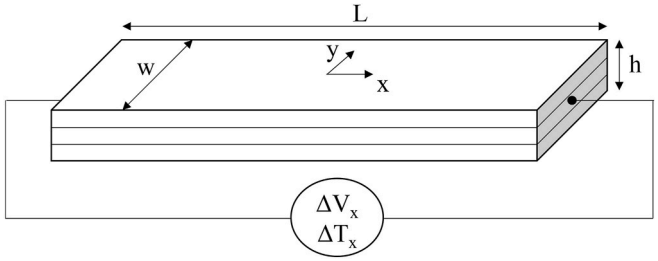

Fig. 4. Schematic of a rectangular specimen.

Considering that g_y and e_y are nearly zero in wide specimens and that $I_x = 0$ (by definition), and further substituting in the first line of Eq. (31), the limit condition for the specimen Seebeck coefficient can be obtained as:

$$s_{x,s}^{0} = -\frac{\Delta V_x}{\Delta T_x} = \frac{A_{xx}\cdot S_{xx} + A_{xy}\cdot S_{yx}}{A_{xx}} \tag{53}$$

For balanced laminates, Eq. (53) leads to S_{xx} only, confirming their insensitivity to the type-I edge effects.

4.3. Type-II edge effects

Different from the type-I, type-II edge effects exist in multidirectional laminates only, not in unidirectional plies. They are due to the different material properties of the stacked layers in the global coordinate system, causing a different ply-by-ply response in proximity of the free edges, as for the mechanical response [26].

Let us consider a rectangular specimen under a voltage or temperature difference along the x-direction (as depicted in Fig. 4); plies with different orientation respond differently to the excitation leading, close to the edges, to a non-uniform through-the-thickness distribution for the y-direction components of the electric field and the thermal gradient. This, in turn, causes out-of-plane fluxes, violating the basic assumptions of the theoretical models developed in Section 2. The size of the region, close to the free edges, where this perturbation has a non-negligible effect is approximatively proportional to the total laminate thickness h. Accordingly, the w/h ratio governs the specimen behaviour in relation to the type-II edge effects.

In particular, in the case of very thin and wide specimens (very large w/h ratio), type-II edge effects can be neglected, as such a perturbation occurs in a very limited region close to edges, and the specimen response is influenced by the L/w ratio only.

Eventually, for very thick specimens (limited w/h ratio), the entire

width is influenced by free edge effects, so that e_y and g_y have a non-homogeneous distribution in the whole specimen. In this condition, the layers act as electric and thermal conductors in parallel along x, whereas they are completely de-coupled along y.

Considering also that the y-direction fluxes are equal to zero in the perturbed regions (and thus, within reason, in the whole specimen), the thick specimen conductivities can be calculated by means of Eqs. (3, 14) imposing $j_y = g_y = 0$ giving:

$$\sigma^t_{x,s} = \frac{I_x}{\Delta V_x}\frac{L}{h} = \frac{1}{h}\sum_{i=1}^{n}\frac{h_i}{\overline{\rho}^i_{xx}} \tag{54}$$

$$k^t_{x,s} = \frac{I_x}{\Delta V_x}\frac{L}{h} = \frac{1}{h}\sum_{i=1}^{n}\frac{h_i}{\overline{r}^i_{11}} \tag{55}$$

where $\overline{r}^i_{xx}$ is the term in position 1,1 of the matrix $[\overline{r}^i] = [\overline{k}^i]^{-1}$.

In order to calculate the apparent thermoelectric behaviour of a specimen with $w/h \cong 0$, the Seebeck coefficient of each i-th layer has to be calculated, imposing $q_y = 0$:

$$s^t_{x,i} = -\frac{\Delta V_x}{\Delta T_x} = \frac{\overline{s}^i_{xx} - \overline{s}^i_{xy}\frac{\overline{\gamma}^i_{xy}\overline{s}^i_{xy}+\overline{k}^i_{xy}+\overline{\delta}^i_{xy}}{\overline{\gamma}^i_{yy}\overline{s}^i_{yy}+\overline{k}^i_{yy}+\overline{\delta}^i_{yy}}}{1+\overline{s}^i_{xy}\frac{\overline{r}^i_{xy}}{\overline{\gamma}^i_{yy}\overline{s}^i_{yy}+\overline{k}^i_{yy}+\overline{\delta}^i_{yy}}} \tag{56}$$

where:

$$[\overline{\gamma}^i] = \begin{bmatrix}\overline{\gamma}^i_{xx} & \overline{\gamma}^i_{xy}\\ \overline{\gamma}^i_{yx} & \overline{\gamma}^i_{yy}\end{bmatrix} = [\overline{\sigma}^i][\overline{s}^i]$$
$$[\overline{\delta}^i] = \begin{bmatrix}\overline{\delta}^i_{xx} & \overline{\delta}^i_{xy}\\ \overline{\delta}^i_{yx} & \overline{\delta}^i_{yy}\end{bmatrix} = \left[\overline{\beta}^i\right][\overline{\sigma}^i][\overline{s}^i] \tag{57}$$

Now, considering that the layers act in parallel along the x-direction and recalling the formulation for the Seebeck coefficient of constituents in parallel reported in Ref. [19], the following expression can be written for the thick specimen Seebeck coefficient:

$$s^t_{x,s} = -\frac{\Delta V_x}{\Delta T_x} = \frac{1}{\sigma^t_{x,s}}\sum_{i=1}^{n}\frac{h_i}{h}\frac{1}{\overline{\rho}^i_{xx}}s^t_{x,i} \tag{58}$$

Eqs. (54)-(58), however, are limit conditions valid for finite values of the L/w ratio only. Indeed, if the experimental measurement is done by using metallic electrodes covering the entire left and right cross-sections in Fig. 4, then the potential in these two faces is uniform along the thickness. If L/w tends to zero, this behaviour can be extended to the whole specimen length, leading to a planarity of the fluxes. Therefore, the limit solution for very wide laminates, Eqs. (48)–(50) can be used, independently of the w/h ratio.

4.4. Concluding remarks on edge effects

As a final remark related to the influence of free-edge effects on the thermoelectric behaviour of composite laminates, it has to be underlined that the expressions reported in Eqs. (48)-(55), (58) represent limit conditions that bound the actual behaviour of specimens with finite dimensions, as proved by parametric FE analyses reported in Appendix B.

In addition to this, it is also worth mentioning that free-edge effects may significantly affect experimental measurements carried out on finite size rectangular coupons with a given stacking sequence, thus making, in some cases, the measured values very different from the bulk thermoelectrical properties of that laminate configuration. This fact is particularly important when moving from laboratory specimens to real components with a wide surface extension, where edge effects are negligible.

Accordingly, in the last-mentioned case, due to the different role played by edge effects, the overall thermoelectric behaviour of the component may be very different from that measured on the laboratory specimen with the same lay-up, and is expected, instead, to be very close to the values obtainable using the models reported in Section 2. Thus, in the engineering practice, the thermoelectrical design of real components, characterized by a wide surface extension, can be directly carried out using the analytical models derived in Section 2.

5. Validation through experiments

5.1. Materials and testing procedures

To experimentally validate the electric and thermoelectric models developed, measurements of the electrical conductivity and the Seebeck coefficient of multi-directional laminates were carried out. Carbon fibres received from Torayca (T700, 12k tow, sizing 60e) in the form of a UD tape with 300 g per square meter (gsm) were adopted. A commercial DGEBA-based epoxy resin and amine-based hardener (LY-5052) by Huntsman Advanced Materials Inc. were used as the CFRP laminate matrix system at a resin to hardener weight ratio of 100:38% w/w. The epoxy/hardener system was mechanically mixed and subsequently degassed for 15 min to reduce the presence of air. Afterwards, it was applied to the carbon fibre tape using a roller followed by a vacuum bagging process and left to cure for 24 h at room temperature. Then, a post-curing was applied by thermo-pressing at 100 °C and 20 bar for a total duration of 4 h. The resulting fibre volume fraction was approximately 0.52. Laminates with different lay-ups were manufactured. First, a UD laminate made of eight 0° plies was produced for obtaining the single ply properties. In addition, 8-ply $[0/90]_{2s}$ and $[45/-45]_{2s}$ laminates were manufactured. The plates were cut with a circular diamond saw into 50 mm × 50 mm specimens for measuring the longitudinal and the transverse electric conductivity and Seebeck coefficient. The final laminate thickness was 2 mm.

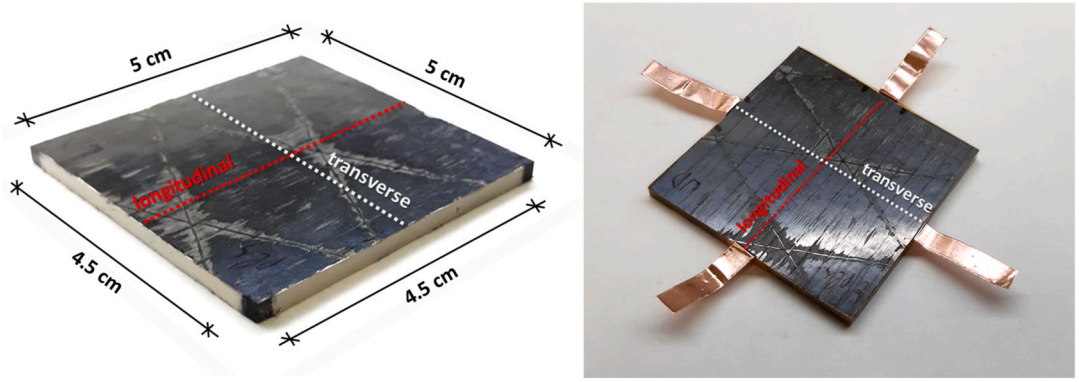

Fig. 5. Schematic illustration of the CFRP sample geometry for the longitudinal and transverse electrical conductivity and Seebeck coefficient measurements, respectively. Representative sample with Cu conductive tape applied for the measurements is shown in the same figure (right hand-side).

Table 2
Comparison between experimental and predicted values of the electric conductivity and Seebeck coefficient (superscript legend: exp = experimental measurement, 0 = narrow specimen limit, ∞ = large specimen limit, t = thick specimen limit).

Lay-up	Direction	Experimental		Simulated			
		σ_s^{exp} (S/m)	s_s^{exp} (μV/K)	$\sigma_s^0 = \sigma_s^\infty = \sigma_x$ (S/m)	σ_s^t (S/m)	$s_s^0 = s_s^\infty = s_x$ (μV/K)	s_s^t (μV/K)
UD (8-ply)	Longitudinal	4545 ± 40	4.01 ± 0.2	–	–	–	–
	Transverse	220 ± 5	4.09 ± 0.2	–	–	–	–
$[0/90]_{2s}$	Longitudinal	2415 ± 18	4.32 ± 0.1	2382	2382	4.01	4.01
	Transverse	2222 ± 24	4.33 ± 0.1	2382	2382	4.01	4.01
$[\pm45]_{2s}$	Longitudinal	2057 ± 20	4.22 ± 0.2	2382	420	4.01	4.06
	Transverse	1915 ± 22	4.23 ± 0.1	2382	420	4.01	4.06

The metallic contacts were obtained by placing a low-temperature and fast curing silver paste (Agar scientific, Germany) on the specimens' cross sections, involving the entire thickness and a width of 45 mm (Fig. 5).

Two-point probe electrical resistance measurements were performed using an Agilent 34401A 6½ digital multimeter (DMM). The distance between the electrodes (50 mm) defined the resistor's length used for the conductivity calculations. From the measured resistance, R = Δv/I, the apparent specimen conductivity was calculated as

$$\sigma_s^{exp} = \frac{L}{R \cdot w \cdot h} \tag{59}$$

where L = 50 mm, w = 45 mm and h = 2 mm.

The longitudinal and transverse Seebeck coefficients of the CFRPs with different lay-ups were measured using a custom-made set-up that has been described in detail in Ref. [27]. In brief, the samples were placed on two metal blocks, which enabled the generation of a temperature gradient (ΔT) along the longitudinal and transverse direction, respectively. For all measurements, one block was kept at room temperature (25 °C) via water circulation, while the other one was heated at 50 °C, 75 °C and 125 °C. The generated voltage drop (Δv) was measured across two electrodes by an Agilent 34401A 6½ digital multimeter. The temperature of the hot and cold sides was constantly measured with K-type thermocouples to determine the exact temperature difference (ΔT), while the Seebeck coefficient (s) was derived by the well-known formula $s_s^{exp} = -\Delta v/\Delta T$. Longitudinal and transverse measurements were carried out for the different CFRP samples.

5.2. Results and discussion

The measured values of the electric conductivity and Seebeck coefficient along the longitudinal and transverse directions are reported in Table 2 and Fig. 6, together with the model predictions for the three limit conditions outlined in Section 4. It is important to remind that all the analysed laminate configurations are not affected by the type-I edge effects as there are, globally, no couplings between longitudinal and transverse gradients and fluxes. For all of them, thus, the L/w ratio does not affect the specimen behaviour, so that the properties related to infinitely narrow and large specimens are the same and correspond to the bulk values. $[\pm45]_{2s}$ laminates are influenced by the type-II edge effects and, therefore, the w/h ratio, which is in this case equal to 22.5. Concerning the electric conductivity, the experimental results for the cross-ply laminate agree well with the predictions. The slight discrepancy between the experimental values of the conductivity along the longitudinal and transverse directions may be due to small differences in the fibre volume fraction between the 0° and 90° layers. Regarding this, we remind that the specimens were not made from commercial prepregs with a fixed V_f, but they were manufactured by impregnating the dry unidirectional fibres. This process could result in small differences in the fibre content, and thus in the electric properties, between different layers.

The conductivity for the $[\pm45]_{2s}$ laminates is slightly over-predicted. This agrees with the fact that this configuration is affected by type-II edge effects, which make the apparent specimen conductivity lower than the bulk one for real specimens with a finite w/h ratio. The conductivity for the infinitely thick specimen is indeed much lower and equal to 420 S/m, as reported in the table. Accordingly, the difference in the measured and predicted values is not due to the inaccuracy of the model, but to edge effects for which only limit solutions can be derived.

Concerning the Seebeck coefficient, a reasonable agreement is obtained between the measured values and the theoretical predictions, given the compatibility of the relevant scatter bands (Table 2).

5.3. Comparison with results from the literature

To provide a further validation of the developed models, the existing literature was analysed to gather experimental results on the electric, thermal and thermoelectric properties of composite laminates. Only results on the electrical properties were found, in Ref. [23], for aligned CNT webs embedded within glass/epoxy laminates. The electrical conductivity along directions 1 and 2 were measured, resulting in σ_1 = 5578 S/m and σ_2 = 226 S/m. Then, laminates with different stacking sequences were considered (see Table 3). The authors used two specimen configurations for the electric measurements, namely large

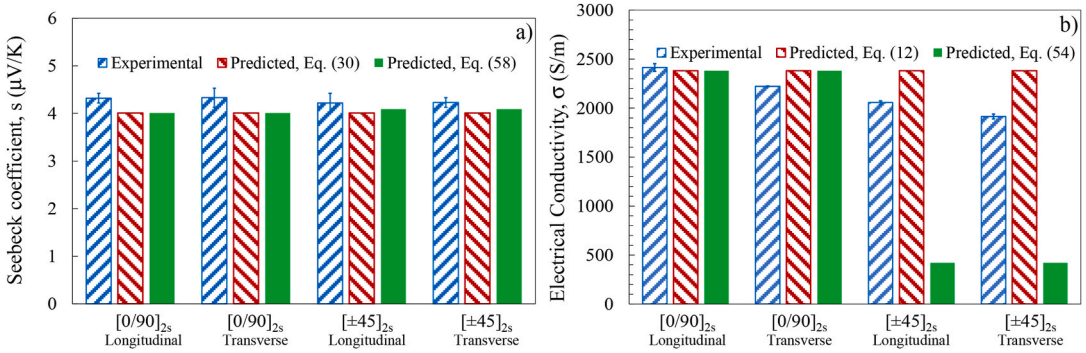

Fig. 6. Comparison between measured and predicted values for a) the Seebeck coefficient and b) the electric conductivity.

Table 3
Comparison between model predictions and the experimental results from Ref. [23] (superscript legend: exp = experimental measurement, 0 = narrow specimen limit, ∞ = large specimen limit, t = thick specimen limit).

	Lay-up	$\sigma_{x,s}^{exp}$ (L/w = 1) (S/m)	$\sigma_{x,s}^{exp}$ (L/w = 4) (S/m)	$\sigma_{x,s}^{0} = \sigma_x$ (S/m)	$\sigma_{x,s}^{\infty}$ (S/m)	$\sigma_{x,s}^{t}$ (S/m)
Unbalanced laminates	45	938	467	2902	434	–
	0/22.5	4878	4237	5186	3737	3413
	0/45	3903	3411	4240	3095	3006
Balanced laminates	0/90	2933	2921	2902	2902	2902
	22.5/-22.5	4732	4759	4794	4794	1248
	45/-45	2784	2710	2902	2902	434
	67.5/-67.5	1078	1089	1010	1010	263
	22.5/-67.5	3060	2978	2902	2902	756
	0/45/-45/90	2984	3017	2902	2902	1668

specimens, with L/w = 1, and narrow specimens, with L/w = 4. The length was kept equal to 40 mm. In both cases, an electric potential difference Δv_x was imposed to the laminates along direction x (corresponding to the 0° oriented CNTs in the lay-up) and the apparent specimen conductivity $\sigma_{x,s}$ was calculated as in Eq. (59).

As a first comment, it can be noted that for the balanced configurations the experimental results for large and narrow specimens are perfectly compatible. This agrees with the fact that such balanced configurations are not affected by the type-I edge effects and their behaviour does not depend on the L/w ratio. It depends, instead, on the w/h ratio, as shown in the last column of the table, where the values calculated for the infinitely thick specimen configuration are reported (see Eqs. (54), (58)). However, in this case the thickness of the conductive CNT webs is of 12 μm only, so that the thick specimen condition is never approached in the tested samples. For these laminate configurations there is a perfect agreement between the experimental results and the theoretical predictions for thin specimens ($\sigma_{x,s}^{0}$ and $\sigma_{x,s}^{\infty}$). The first three rows are related to unbalanced configurations, for which type-I edge effects are relevant. The experimental results are always included within the limit values for infinitely narrow and infinitely large specimens. In particular, the conductivities for L/w = 1 are closer to those predicted for infinitely large specimens ($\sigma_{x,s}^{0}$). Conversely, those for L/w = 4 tend towards the predictions for infinitely narrow specimens ($\sigma_{x,s}^{\infty}$). It is worth reminding that type-II edge effects are not present in the unidirectional 45° configuration, so that its behaviour does not depend on the w/h ratio.

6. Conclusions

Exact analytical models were developed for estimating the in-plane electric, thermal and thermoelectric properties of multidirectional composite laminates. The full thermoelectric coupled constitutive law for a generic laminate was also obtained. The developed models were successfully validated through Finite Element analyses on representative laminate segments under periodic boundary conditions. The occurrence of edge effects in rectangular specimens with finite dimensions used for measuring the laminate properties was also discussed, identifying three limit conditions: infinitely narrow, infinitely large and infinitely thick specimen. For each of them, the apparent values of the electric and thermal conductivities and Seebeck coefficient were obtained.

Eventually, an experimental validation was carried out comparing the results from the developed analytical expressions with a set of new experimental results obtained from carbon/epoxy square specimens with different stacking sequences. In addition, as a further step of validation of the electrical model and the identified edge effects, experimental data taken from the literature were reconsidered and compared with the analytical predictions, showing a very satisfactory agreement.

As a final concluding remark, the developed models represent a very useful tool for designing the laminate configuration, including the lay-up and the geometry, to meet a specific target in thermoelectric applications.

Author statement

I certify that the article is the author' original work, it hasn't received prior publication and it isn't under consideration for publication elsewhere.

Declaration of competing interest

The authors declare that they have no known competing financial interests or personal relationships that could have appeared to influence the work reported in this paper.

Acknowledgements

This work has been carried out within the frame of the EU-funded project "Hierarchical multifunctional composites with thermoelectrically powered autonomous structural health monitoring for the aviation industry (HARVEST)", H2020 Grant Agreement Number 769140.

APPENDIX A

The aim of this appendix is to provide the reader with evidence of the flux planarity in the bulk regions of a laminate, i.e. far from the edges, this being a fundamental hypothesis for the analytical derivation of the bulk laminate properties in Section 2. As an example, a 3D electric FE analysis of a rectangular specimen with L = 50 mm, w = 10 mm, h = 2 mm was carried out (see the schematic in Fig. A1). The lay-up was [0/45] and the ply electric conductivities were $\sigma_1 = 4545$ S/m and $\sigma_2 = 220$ S/m, as reported in Table 2, relevant to the material tested in this work. A zero Volt potential was applied to the whole left face, whereas a 1 V potential was assigned to the right one. No periodic boundary conditions were applied, to simulate the behaviour of a specimen with two electrodes on its ends, covering the entire cross-sections.

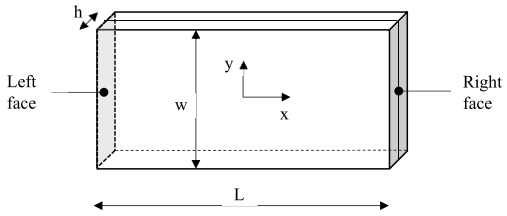

Fig. A1. Schematic of the specimen geometry for the 3D FE analyses.

Fig. A2 shows the contour plot of the electric potential. In the left part of the figure, it can be seen that the potential varies in the laminate plane, but also along the thickness in correspondence of the edges. In the right part of the figure, the contour plot in a single section of the specimen is shown. The through-the-thickness variation of the potential involves a region in proximity of the edges only, whereas in the central part the two plies have the same potential value, leading to the planarity of the current densities. The extension of the perturbed zone extends from the edges of a length that depends on the laminate thickness and the material properties, but the iso-potential condition is always reached in the central part of the laminate, provided that it is wide enough.

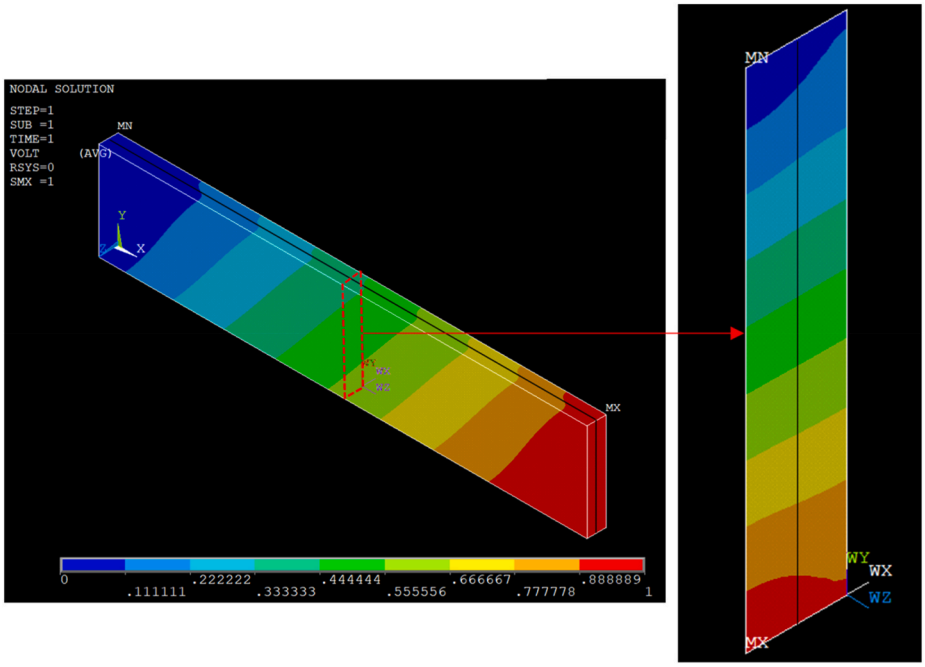

Fig. A2. Electric potential contour plot for a [0/45] specimen.

APPENDIX B

In this appendix, the results of parametric FE analyses on specimens with different geometrical ratios L/w and w/h are shown, in comparison with the limit conditions predicted by the analytical formulations derived in Section 4 for the edge effects. As the electric and thermal problems are formally identical, only electric and thermoelectric analyses were carried out. The longitudinal and transverse material properties were those listed in Table 2, with the addition of the thermal conductivities reported in Table 1, typical of carbon/epoxy UD composites. Again, the out-of-plane properties were considered equal to the transverse ones.

Parallelepiped specimens with the geometry shown in Fig. A1 were modelled, considering [45/-45] and [0/45] laminates configurations, as representative cases of type II and mixed I-II edge effects, respectively. With reference to the schematic in Fig. A1, electric analyses were carried out by imposing a potential value of 0 and 1 V on the left and right faces, respectively.

The apparent specimen conductivity was then calculated as

$$\sigma_{x,s} = \frac{\sum_{i=1}^{n} j_{xi} \times Vol_i}{\sum_{i=1}^{n} Vol_i} \cdot \frac{L}{\Delta v} \tag{B.1}$$

where j_{xi} and Vol_i are the x direction current density and the volume of the i-th element, respectively, whereas the potential drop Δv is equal to 1 V, as imposed through the boundary conditions.

In the thermoelectric analyses, the temperature was fixed at 293 K and 294 K on the left and right faces, respectively. In addition, a zero Volt potential was assigned to the left face and the electric potential was imposed to be uniform (but not known) in the entire right face, simulating the

presence of an electrode. The specimen Seebeck coefficient was then calculated as

$$s_{x,s} = -\frac{\Delta v}{\Delta T} = -\frac{v_{right}}{\Delta T} \tag{B.2}$$

where v_{right} is the potential of any of the nodes on the right face and ΔT is equal to 1 K, as imposed through the boundary conditions.

The element size was chosen to ensure the convergency of the results.

Fig. B1 shows the results obtained for the [45/-45] laminate with a fixed L/w ratio equal to 5 and different w/h ratios. It is worth reminding that this laminate configuration is affected by type-II edge effects only, associated to the width to thickness ratio. Both the specimen conductivity and Seebeck coefficient tend to the limit conditions of the thick laminate for low w/h ratios. As the latter is increased, the properties approach those obtained for narrow or wide specimens, which are equal to the bulk properties, the laminate being balanced.

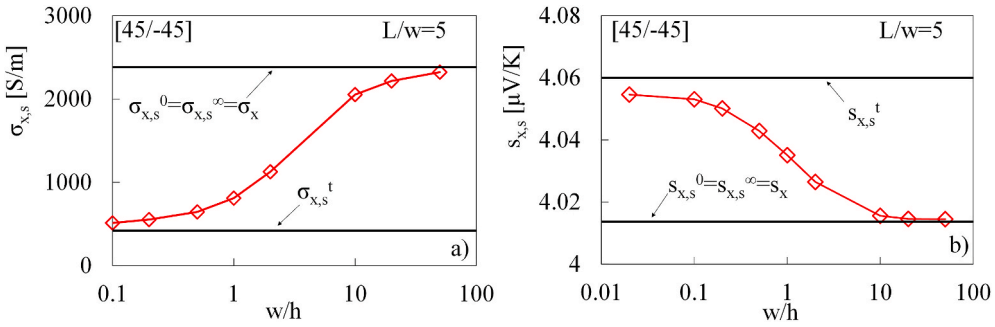

Fig. B1. Influence of the w/h ratio on the a) electric conductivity and b) Seebeck coefficient of a [45/-45] specimen.

In Fig. B2, the influence of the L/w ratio is shown for the same laminate lay-up, with a fixed w/h = 0.1, corresponding to a very thick specimen. As mentioned in Section 4.3, the limit condition for the thick specimen is only reached for finite values of L/w (>0), so that this ratio influences the entity of the type-II edge effects as well. Accordingly, the specimen properties shown in Fig. B2 tend to the thick specimen limit for increasing values of L/w and to the bulk properties for L/w→0.

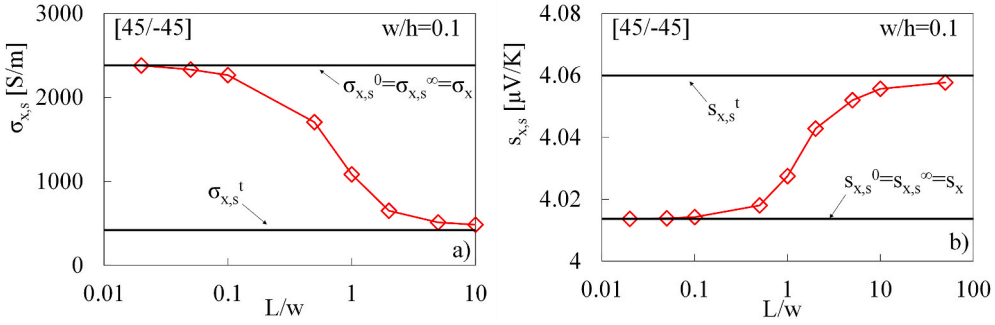

Fig. B2. Influence of the L/w ratio on the a) electric conductivity and b) Seebeck coefficient of a [45/-45] specimen.

The behaviour of [0/45] laminates is more complex as it is affected by both type-I and II edge effects. To highlight the influence of type-I edge effects, a thin laminate configuration is first chosen (w/h = 10), varying the L/w ratio. The results, shown in Fig. B3, confirm that the specimen properties approach the limit conditions for narrow and wide specimens as L/w tends to ∞ and zero, respectively.

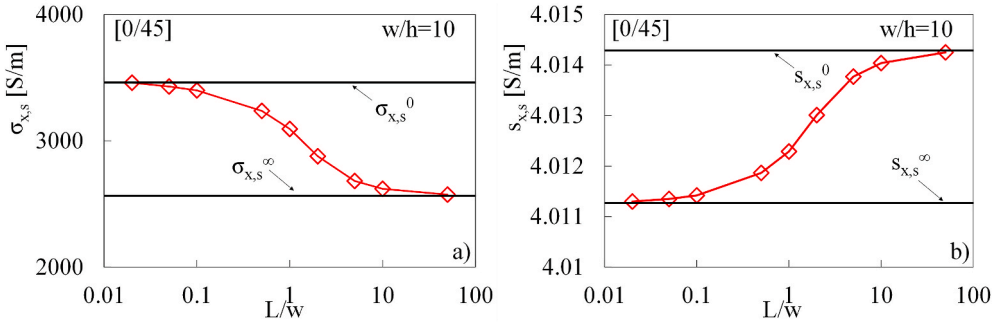

Fig. B3. Influence of the L/w ratio on the a) electric conductivity and b) Seebeck coefficient of a [0/45] specimen.

The influence of type-II edge effects for the [0/45] laminate is eventually shown in Fig. B4, where the effect of the w/h and L/w ratios is simultaneously presented. Let us consider, first, the condition with L/w = 10 (narrow specimen). As expected, the properties tend to the thick specimen limit as w/h approaches zero. As this ratio is increased, the specimen properties change and saturate to a value that is different from that of both the infinitely narrow and wide specimen. This value is, indeed, dependant of the L/w ratio as it is affected by type-I edge effects.

Decreasing L/w, the asymptote for w/h→0 increases, progressively reaching the wide specimen limit as L/w→0, as already discussed in section 4.3.

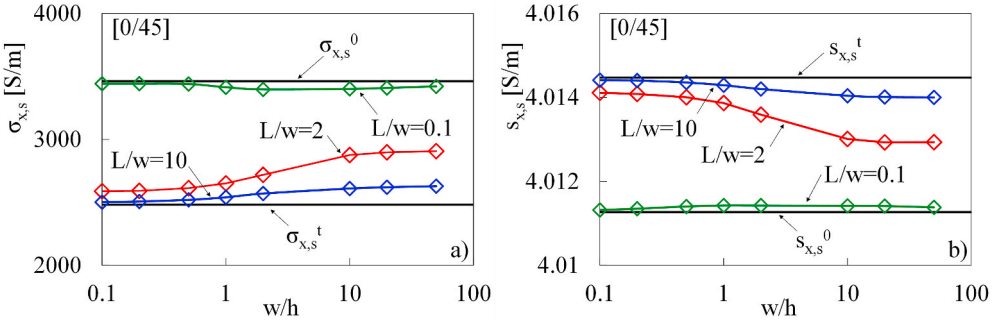

Fig. B4. Combined influence of the L/w and w/h ratios on the a) electric conductivity and b) Seebeck coefficient of a [0/45] specimen.

The results presented in this appendix represent a validation of the limit conditions identified in section 4, and, most important, shed light onto the importance of edge effects when measuring the electric and thermoelectric properties of a laminate through a finite size specimen. Care has to be taken when considering such measured values which are not relevant to the bulk laminate but are, in fact, specimen properties.

References

[1] K. Schulte, C. Baron, Load and failure analyses of CFRP laminates by means of electrical resistivity measurements, Compos. Sci. Technol. 36 (1989) 63–76, https://doi.org/10.1016/0266-3538(89)90016-X.

[2] P.E. Irving, C. Thiagarajan, Fatigue damage characterization in carbon fibre composite materials using an electrical potential technique, Smart Mater. Struct. 7 (1998) 456, https://doi.org/10.1088/0964-1726/7/4/004.

[3] S. Wang, D.D.L. Chung, Self-sensing of flexural strain and damage in carbon fiber polymer-matrix composite by electrical resistance measurement, Carbon 44 (2006) 2739–2751, https://doi.org/10.1016/j.carbon.2006.03.034.

[4] A. Todoroki, K. Omagari, Y. Shimamura, H. Kobayashi, Matrix crack detection of CFRP using electrical resistance change with integrated surface probes, Compos. Sci. Technol. 66 (2006) 1539–1545, https://doi.org/10.1016/J.COMPSCITECH.2005.11.029.

[5] L. Böger, M.H.G. Wichmann, L.O. Meyer, K. Schulte, Load and health monitoring in glass fibre reinforced composites with an electrically conductive nanocomposite epoxy matrix, Compos. Sci. Technol. 68 (2008) 1886–1894, https://doi.org/10.1016/J.COMPSCITECH.2008.01.001.

[6] T.W. Chou, L. Gao, E.T. Thostenson, Z. Zhang, J.H. Byun, An assessment of the science and technology of carbon nanotube-based fibers and composites, Compos. Sci. Technol. 70 (2010) 1–19, https://doi.org/10.1016/J.COMPSCITECH.2009.10.004.

[7] M. Zappalorto, F. Panozzo, P.A. Carraro, M. Quaresimin, Electrical response of a laminate with a delamination: modelling and experiments, Compos. Sci. Technol. 143 (2017) 31–45, https://doi.org/10.1016/J.COMPSCITECH.2017.02.023.

[8] L. Tzounis, M. Zappalorto, F. Panozzo, K. Tsirka, L. Maragoni, A.S. Paipetis, M. Quaresimin, Highly conductive ultra-sensitive SWCNT-coated glass fiber reinforcements for laminate composites structural health monitoring, Compos. B Eng. 169 (2019) 37–44, https://doi.org/10.1016/J.COMPOSITESB.2019.03.070.

[9] F. Panozzo, M. Zappalorto, L. Maragoni, S.K. Nothdurfter, A. Rullo, M. Quaresimin, Modelling the electrical resistance change in a multidirectional laminate with a delamination, Compos. Sci. Technol. 162 (2018) 225–234, https://doi.org/10.1016/J.COMPSCITECH.2018.04.031.

[10] G. Karalis, L. Tzounis, E. Lambrou, L.N. Gergidis, A.S. Paipetis, A carbon fiber thermoelectric generator integrated as a lamina within an 8-ply laminate epoxy composite: efficient thermal energy harvesting by advanced structural materials, Appl. Energy 253 (2019) 113512, https://doi.org/10.1016/J.APENERGY.2019.113512.

[11] E.J.X. Pang, S.J. Pickering, A. Chan, K.H. Wong, P.L. Lau, N-type thermoelectric recycled carbon fibre sheet with electrochemically deposited Bi2Te3, J. Solid State Chem. 193 (2012) 147–153, https://doi.org/10.1016/J.JSSC.2012.04.046.

[12] S. Han, D.D.L. Chung, Through-thickness thermoelectric power of a carbon fiber/epoxy composite and decoupled contributions from a lamina and an interlaminar interface, Carbon 52 (2013) 30–39, https://doi.org/10.1016/J.CARBON.2012.08.071.

[13] D.H. Sung, G.H. Kang, K. Kong, M. Kim, H.W. Park, Y. Bin Park, Characterization of thermoelectric properties of multifunctional multiscale composites and fiber-reinforced composites for thermal energy harvesting, Compos. B Eng. 92 (2016) 202–209, https://doi.org/10.1016/J.COMPOSITESB.2016.02.050.

[14] M. Kim, D.H. Sung, K. Kong, N. Kim, B.J. Kim, H.W. Park, Y. Bin Park, M. Jung, S. H. Lee, S.G. Kim, Characterization of resistive heating and thermoelectric behavior of discontinuous carbon fiber-epoxy composites, Compos. B Eng. 90 (2016) 37–44, https://doi.org/10.1016/J.COMPOSITESB.2015.11.037.

[15] D.J. Bergman, O. Levy, Thermoelectric properties of a composite medium, J. Appl. Phys. 70 (1991) 6821, https://doi.org/10.1063/1.349830.

[16] L. Liu, A continuum theory of thermoelectric bodies and effective properties of thermoelectric composites, Int. J. Eng. Sci. 55 (2012) 35–53, https://doi.org/10.1016/J.IJENGSCI.2012.02.003.

[17] P. Wang, B.L. Wang, K.F. Wang, H. Hirakata, C. Zhang, Analysis of three-dimensional ellipsoidal inclusions in thermoelectric solids, Int. J. Eng. Sci. 142 (2019) 158–169, https://doi.org/10.1016/J.IJENGSCI.2019.06.005.

[18] J. Jung, S. Lee, B. Ryu, S. Ryu, Investigation of effective thermoelectric properties of composite with interfacial resistance using micromechanics-based homogenisation, Int. J. Heat Mass Tran. 144 (2019) 118620, https://doi.org/10.1016/J.IJHEATMASSTRANSFER.2019.118620.

[19] P.A. Carraro, L. Maragoni, A.S. Paipetis, M. Quaresimin, L. Tzounis, M. Zappalorto, Prediction of the Seebeck coefficient of thermoelectric unidirectional fibre-reinforced composites, Compos. B Eng. 223 (2021) 109111, https://doi.org/10.1016/J.COMPOSITESB.2021.109111.

[20] M. Zappalorto, P.A. Carraro, R. Pietrogrande, M. Quaresimin, Modelling the electrical resistance of multidirectional laminates with off-axis cracks, Compos. Struct. 237 (2020) 111928, https://doi.org/10.1016/J.COMPSTRUCT.2020.111928.

[21] D.P.H. Hasselman, H. Bhatt, K.Y. Donaldson, J.J.R. Thomas, Effect of fiber orientation and sample geometry on the effective thermal conductivity of a uniaxial carbon fiber-reinforced glass matrix composite, J. Compos. Mater. 26 (1992) 2278–2288, https://doi.org/10.1177/002199839202601506.

[22] M.R. Kulkarni, R.P. Brady, A model of global thermal conductivity in laminated carbon/carbon composites, Compos. Sci. Technol. 57 (1997) 277–285, https://doi.org/10.1016/S0266-3538(96)00116-9.

[23] X. Yao, B.G. Falzon, S.C. Hawkins, Orthotropic electro-thermal behaviour of highly-aligned carbon nanotube web based composites, Compos. Sci. Technol. 170 (2019) 157–164, https://doi.org/10.1016/J.COMPSCITECH.2018.11.042.

[24] E.C. Senis, I.O. Golosnoy, J.M. Dulieu-Barton, O.T. Thomsen, Enhancement of the electrical and thermal properties of unidirectional carbon fibre/epoxy laminates through the addition of graphene oxide, J. Mater. Sci. 54 (2019) 8955–8970, https://doi.org/10.1007/S10853-019-03522-8.

[25] E.J. Barbero, Introduction to Composite Materials Design, second ed., CRC Press, Boca Raton, 2010 https://doi.org/10.1201/9781315296494.

[26] R.B. Pipes, N.J. Pagano, Interlaminar stresses in composite laminates under uniform axial extension, J. Compos. Mater. 4 (1970) 538–548.

[27] C.K. Mytafides, L. Tzounis, G. Karalis, P. Formanek, A.S. Paipetis, High-power all-carbon fully printed and wearable SWCNT-based organic thermoelectric generator, ACS Appl. Mater. Interfaces 13 (2021) 11151–11165, https://doi.org/10.1021/ACSAMI.1C00414.